



Published in final edited form as:

Oncogene. 2018 August ; 37(32): 4413–4427. doi:10.1038/s41388-018-0227-y.

HRI-mediated translational repression reduces proteotoxicity and sensitivity to bortezomib in human pancreatic cancer cells

Matthew C. White^{1,2,3}, Rebecca D. Schroeder³, Keyi Zhu^{1,2}, Katherine Xiong^{1,2}, and David J. McConkey^{1,2,3}

¹Department of Urology, The University of Texas MD Anderson Cancer Center, Houston, TX 77030

²Department of Cancer Biology, The University of Texas MD Anderson Cancer Center, Houston, TX 77030

³Program in Experimental Therapeutics, The University of Texas Graduate School of Biomedical Sciences, Houston, TX 77030

Abstract

Human cancer cells display extensive heterogeneity in their sensitivities to the proteasome inhibitor bortezomib (Velcade). The molecular mechanisms underlying this heterogeneity remain unclear, and strategies to overcome resistance are limited. Here, we discover that inherent differences in eIF2 α phosphorylation among a panel of 10 human pancreatic cancer cell lines significantly impacts bortezomib sensitivity, and implicate the HRI (heme-regulated inhibitor) eIF2 α kinase as a novel therapeutic target. Within our panel, we identified a subset of cell lines with defective induction of eIF2 α phosphorylation, conferring a high degree of sensitivity to bortezomib. These bortezomib-sensitive cells exhibited impaired translation attenuation followed by toxic accumulation of protein aggregates and reactive oxygen species (ROS), whereas the bortezomib-resistant cell lines displayed increased phosphorylation of eIF2 α , decreased translation, few protein aggregates, and minimal ROS production. Importantly, we identified HRI as the primary bortezomib-activated eIF2 α kinase, and demonstrated that HRI knockdown promoted cell death in the bortezomib-resistant cells. Overall, our data implicate inducible HRI-mediated phosphorylation of eIF2 α as a central cytoprotective mechanism following exposure to bortezomib and provide proof-of-concept for the development of HRI inhibitors to overcome proteasome inhibitor resistance.

Keywords

Proteasome inhibition; bortezomib; proteotoxic stress; oxidative stress; eIF2 α ; translation; HRI

Users may view, print, copy, and download text and data-mine the content in such documents, for the purposes of academic research, subject always to the full Conditions of use: http://www.nature.com/authors/editorial_policies/license.html#terms

Address correspondence to: David J. McConkey, Ph.D., Johns Hopkins Greenberg Bladder Cancer Institute, Marburg 149, 600 North Wolfe Street, Baltimore, MD 21287, djmconkey@jhmi.edu.

Supplementary Information accompanies the paper on the *Oncogene* website (<http://www.nature.com/onc>).

INTRODUCTION

The ubiquitin-proteasome system (UPS) is responsible for the majority of intracellular protein degradation (1, 2). Inhibition of the proteasome causes significant intracellular buildup of misfolded proteins that are prone to aggregation and results in the activation of multiple protein quality-control mechanisms that include phosphorylation of the eukaryotic initiation factor 2 at the α subunit (eIF2 α) (3, 4), and activation of the unfolded protein response (UPR) (5), the heat shock response (6), and the autophagy-lysosomal system (7). Of these, eIF2 α phosphorylation is the most upstream mechanism employed by mammalian cells to maintain proteostasis. In the absence of stress, GTP-bound eIF2 binds Met-tRNA_i, forming part of the 43S preinitiation complex and ensuring translation initiation. Upon stress-induced phosphorylation of eIF2's α subunit, eIF2 becomes an inhibitor of eIF2B, preventing eIF2B-induced nucleotide exchange and shutting off cap-dependent translation (8). This global translational arrest and selective upregulation of cytoprotective transcription factors such as ATF4, are collectively referred to as the integrated stress response (ISR) (9). Four kinases, heme-regulated inhibitor (HRI), protein kinase RNA (PKR), protein kinase RNA-like endoplasmic reticulum kinase (PERK), and general control nonderepressible 2 (GCN2) are known to directly phosphorylate eIF2 α in response to heme-deficiency (10), viral double-stranded RNA (11), misfolded proteins in the endoplasmic reticulum (ER) (12), and amino acid depletion (13), respectively. Thus, the eIF2 α kinases sense multiple upstream stressors (14) but propagate the same downstream signal, highlighting the importance of eIF2 α phosphorylation as a stress response hub.

Because preventing misfolded protein accumulation is fundamental to maintaining cell viability, considerable attention is being focused on modulating proteostasis as a therapeutic strategy (15). For example, a large body of evidence implicates the accumulation of protein aggregates in a variety of different neurodegenerative diseases (16), so it may be possible to inhibit the progression of these diseases by promoting misfolded protein degradation. Conversely, cancers derived from tissues with high protein secretory capacities (i.e., the plasma cell neoplasm multiple myeloma (MM) and some pancreatic tumors) may be vulnerable to proteasome inhibitors and other agents that prevent the degradation of misfolded proteins. Furthermore, many of the biological mechanisms that are universally involved in cancer progression, including increased proliferation, Myc activation, aneuploidy, Ras signaling, and oxidative stress, further enhance proteotoxicity (15, 17–19). Proteasome inhibitors are clinically effective in MM and relapsed or refractory mantle cell lymphomas, where bortezomib (Velcade) has received FDA approval and is now the backbone of frontline therapy (20, 21).

We previously reported that the cytotoxic activities of proteasome inhibitors could be augmented by interfering with the handling of ubiquitylated protein aggregates - either via pharmacologic disruption of cytoprotective structures known as aggresomes (22) or inhibition of the autophagy-lysosomal system (7). In the course of these studies we noted marked heterogeneity among cancer cells with regard to their sensitivities to proteasome inhibitor-induced cell death (23). Here we show that among a panel of human pancreatic cancer cells, a subset of cell lines displays defective induction of eIF2 α phosphorylation and delayed translational arrest in response to the proteasome inhibitor bortezomib. This leads to

an accumulation of ubiquitylated protein aggregates and reactive oxygen species (ROS) that precipitates cell death. A separate group of more resistant cells displays intact eIF2 α phosphorylation, which prevents accumulation of protein aggregates and ROS. Our data identify HRI as the predominant bortezomib-activated eIF2 α kinase in the resistant cells and provide a rationale for exploring it as a novel therapeutic target.

RESULTS

Heterogeneous effects of bortezomib on cell death and eIF2 α phosphorylation in pancreatic cancer cells

We previously observed significant heterogeneity among human pancreatic cancer cell lines in the levels of apoptosis induced by proteasome inhibitors (22). Here we examined a new panel of cells to determine their sensitivities to a clinically relevant concentration of bortezomib (BZ) using a plasma membrane integrity assay (PI-uptake) that measures cumulative cell death. Immortalized normal pancreatic ductal epithelium cells (HPDE) were used as a control and were relatively resistant to BZ, as was reported previously using DNA fragmentation assays (22). Among the cancer cells we observed a wide range of responses indicative of heterogeneity in drug sensitivities (Fig. 1A). We performed time course experiments to measure eIF2 α phosphorylation in two drug-sensitive (CF-Pac1, T3M4) and two drug-resistant (mPanc96, Suit2) cell lines. Neither BZ nor the ER stress-inducing agent thapsigargin (TG) stimulated increases in eIF2 α phosphorylation in the sensitive cell lines, whereas both compounds promoted strong increases in the resistant lines (Fig. 1B). We then compared the effects of BZ and TG on eIF2 α phosphorylation in the rest of the cell lines in the panel. Overall, across all cell lines, there appeared to be a correlation between defective inducible eIF2 α phosphorylation and BZ sensitivity (Fig. 1B,C), given that only two of the cell lines that exhibited intermediate drug sensitivities (L3.6pl and Panc1) were ranked out of order in the drug sensitivity hierarchy (Fig. 1C). However, correlation calculations between P-eIF2 α levels and BZ sensitivity did not achieve statistical significance, despite regression lines trending toward a positive association between higher P-eIF2 α levels (absolute and fold change) and BZ resistance (Supplemental Fig. 1). Interestingly, a similar pattern did not appear to exist with thapsigargin sensitivity (Supplemental Fig. 2). To more directly determine the contribution of eIF2 α phosphorylation to cell death, we compared the effects of BZ in MEFs expressing either wild-type (51SS) or knock-in mutant (51AA) forms of eIF2 α . The mutant 51AA cells were significantly more sensitive to BZ than the wild-type 51SS cells (Fig. 1D).

Effects of bortezomib on translation, protein aggregation, and oxidative stress

We hypothesized that lack of inducible eIF2 α phosphorylation might prevent efficient translation attenuation leading to a toxic accumulation of misfolded protein aggregates. To test this hypothesis, we utilized a L-[4,5-³H(N)] leucine incorporation assay to measure rates of protein synthesis in cells exposed to BZ. The results (Fig. 2A) confirmed that translation attenuation was delayed in the BZ-sensitive cell lines, which continued incorporating leucine into protein at 100% of control levels for up to 8 hours after BZ exposure, whereas the resistant cells down-regulated translation much earlier (2–4 hours). ³H-leucine incorporation did decrease in BZ-sensitive cells at later timepoints, potentially

due to alternative, eIF2 α -independent mechanisms (24) since eIF2 α phosphorylation never increased in the cells (data not shown). The results were not related to differences in the basal protein synthesis rates among sensitive and resistant cells (Fig. 2B, left panel). The sensitivity of the assay was also validated using the direct translation inhibitor cycloheximide (CHX), which caused similar levels of translational inhibition in all of the cell lines (Fig. 2B, right panel).

We then compared the time-dependent effects of BZ on the accumulation of ubiquitin-positive aggregates in the bortezomib-sensitive CF-Pac1 and T3M4 and the bortezomib-resistant mPanc96 and Suit2 cells using anti-ubiquitin immunofluorescence microscopy. Time course studies revealed that ubiquitin-positive aggregates were readily observed in the drug-sensitive cells by 12 hours (Fig. 2C), whereas few aggregates were present in either of the BZ-resistant cells at the same time point (Fig. 3A). To confirm these results with a different method, we used a variation of a detergent-insoluble protein aggregates assay reported previously (25). Again, BZ induced higher levels of ubiquitin-positive insoluble protein aggregates in the CF-Pac1 and T3M4 as compared to the mPanc96 or Suit2 cells (Fig. 3B). Because protein misfolding and aggregation have been implicated in the production of ROS (26–29), it seemed reasonable that ROS production might contribute to the protein aggregate-associated toxicity of BZ in pancreatic cancer cells. To test this idea, we measured BZ-induced intracellular peroxide production using 2',7'-dichlorodihydrofluorescein diacetate (H₂DCFDA) (30). Bortezomib induced significant rightward shifts in H₂DCFDA fluorescence, indicating increased production of ROS, in the drug-sensitive BxPC3, CF-Pac1 and T3M4 cells, whereas in the drug-resistant mPanc96, Suit2, and MiaPaCa-2 cell lines it did not (Fig. 3C).

Bortezomib-induced protein aggregation and oxidative stress mediate cell death

To explore whether a causal link existed between protein aggregation and cell death, we pre-incubated BZ-sensitive cells with CHX prior to exposing them to BZ and then examined the effects on BZ-induced protein aggregation and cell death. Immunofluorescence confirmed that CHX prevented BZ-induced protein aggregation in CF-Pac1 cells (Fig. 4A), and CHX also prevented BZ-induced death in the CF-Pac1 and T3M4 cells (Fig. 4B). To examine whether protein aggregation was tied to ROS production, we pre-incubated the BZ-sensitive CF-Pac1 cells with CHX and measured H₂DCFDA fluorescence (Fig. 4C). Pre-incubation with CHX almost completely ablated the rightward H₂DCFDA peak shift caused by BZ, indicating that translation attenuation prevented ROS production. To explore whether protein aggregates induced cell death by ROS-mediated mechanisms, we examined the effects of the thiol antioxidant *N*-acetyl-L-cysteine (NAC) on ROS production and cell death. Consistent with our hypothesis, NAC prevented both BZ-induced ROS production and cell death (Fig. 4D).

GCN2 controls constitutive phosphorylation of eIF2 α

We noticed that most of the BZ-sensitive cell lines had elevated levels of phospho-eIF2 α at baseline (Fig. 1A–C). We confirmed this by immunoblotting (Fig. 7B, left panel), and the differences between sensitive (CF-Pac1, T3M4) and resistant (mPanc96, Suit2) cells were significant (Fig. 5A, right panel). To identify the responsible kinase, we used RNAi to knock

down expression of the eIF2 α kinases, HRI, GCN2, and PERK in the CF-Pac1 cells and examined phospho- and total-eIF2 α levels by immunoblotting (Fig. 5B, left panel). We confirmed these results in a separate, sensitive cell line, BxPC3 (Fig. 5B, right panel). The results revealed that GCN2 knockdown resulted in a significant reduction in basal phospho-eIF2 α levels, whereas knockdown of the other kinases or transfection with a non-targeting control had no effect.

Identification of BZ-activated eIF2 α kinase(s)

To better understand the BZ-induced stress response, we measured biomarkers associated with either cytosolic (Hsp72) or ER (Grp78, CHOP) stress responses. Surprisingly, BZ upregulated Hsp72 mRNA levels much more potently than it upregulated either Grp78 or CHOP (Fig. 5C). Thus, it seemed likely that a cytosolic eIF2 α kinase (rather than PERK) might be primarily responsible for the BZ-induced eIF2 α phosphorylation observed in the resistant cells. To directly test this possibility, we examined the concentration-dependent effects of BZ on activation of HRI, PERK, and GCN2 by immunoblotting. As positive controls we used amino acid starvation (leucine deprivation) and ER-stress (TG) to induce activation of GCN2 and PERK, respectively. We monitored GCN2 activation using a phospho-specific antibody, and we measured HRI and PERK activation indirectly by monitoring the appearance of slower migrating species of the kinases by SDS-PAGE and immunoblotting (because the commercially available phospho-specific PERK and HRI antibodies were not as reliable). Bortezomib caused dramatic HRI mobility shifts in the Suit2 cells (Fig. 5D, left panel), whereas it induced more modest effects on PERK, especially when compared to the effects of TG (Fig. 5D). Neither BZ nor TG caused any change in GCN2 phosphorylation (Fig. 5D). Importantly, a similar kinase activation pattern was seen in the BZ-sensitive CF-Pac1 cells (Fig. 5D, right panel). Basal mRNA expression levels of all four kinases were roughly similar, with HRI and GCN2 expression being slightly higher in BZ-sensitive lines; however, none of the kinases were significantly upregulated by BZ (data not shown).

Inhibition of HRI sensitizes cells to bortezomib

Our overall hypothesis was that BZ-induced eIF2 α phosphorylation would be cytoprotective because of decreased translation, protein aggregation, and ROS production. As a final test of this hypothesis, we examined whether transient and/or stable knockdown of the eIF2 α kinase(s) responsible for BZ-induced eIF2 α phosphorylation would sensitize cells to BZ (Fig. 6A–C). Based on the kinase activation data (Fig. 5D), we expected that knockdown of HRI, and to a lesser extent PERK, would promote cell death. Consistent with our expectations, transient siRNA-mediated HRI knockdown strongly promoted BZ-induced cell death in two resistant cell lines (Suit2, MiaPaCa-2). Transient PERK knockdown produced some sensitization but less than HRI knockdown. GCN2 and PKR transient knockdown also modestly increased cell death over the non-targeting control, but the differences were not statistically significant (Fig. 6A–B). To further credential HRI as a potential target, we stably transduced the Suit2 cells with lentiviral vectors containing either nonspecific, shHRI, or shGCN2 constructs (Fig. 6C). Consistent with the results from the siRNA experiments, stable knockdown of HRI produced greater increases in BZ sensitivity than did GCN2 or control knockdown (Fig. 6C, left panel). To characterize the mechanistic consequences of

HRI knockdown, we compared BZ-induced ATF4, phospho- and total-eIF2 α protein levels in the Suit2 cells that had been stably transduced with nonspecific or HRI-specific shRNA constructs (Fig. 6D). Consistent with our expectations, HRI knockdown reduced BZ-induced eIF2 α phosphorylation and led to a striking reduction in BZ-induced ATF4 accumulation. Accordingly, BZ induced higher levels of ubiquitin-positive aggregates in detergent-insoluble fractions of HRI knockdown cells than in the nonspecific vector-transduced controls (Fig. 6E). Together, the results strongly support the conclusion that HRI-mediated eIF2 α phosphorylation inhibited BZ-induced cell death by preventing toxic protein aggregation (Fig. 7).

DISCUSSION

Cancer is characterized by both intra- and inter-tumoral heterogeneity that influences therapeutic efficacy. Understanding the biological mechanisms underlying this heterogeneity is critical to informing future treatment decisions. Here, we demonstrate that defective induction of eIF2 α -phosphorylation contributes to sensitivity to the proteasome inhibitor bortezomib in a subset of human pancreatic cancer cells. In the most sensitive cells, cell death appears to occur because defective eIF2 α phosphorylation results in inefficient downregulation of protein synthesis and a toxic accumulation of ubiquitylated protein aggregates and ROS, whereas BZ-resistant cells possess an intact phospho-eIF2 α response (see overall model in Fig. 7). Although a previous study concluded that eIF2 α phosphorylation contributed positively to proteasome inhibitor-induced cell death (3), our data support the opposite conclusion and are more consistent with the results of a genome-wide siRNA screen in which silencing of key translation initiation factors (*EIF4E*, *EIF4G1*) protected cancer cells from BZ-induced death (31). A proteotoxicity-based mechanism of action for proteasome inhibitors is also supported by studies in MM models that implicated high levels of immunoglobulin synthesis as primary determinants of sensitivity to proteasome inhibitors (32), and an intact phospho-eIF2 α response in resistance (33). Recent work in glioma revealed that expression of a dominant negative eIF2 α mutant sensitized glioma cells to bortezomib and other chemotherapeutic agents, further supporting our findings (34). Accumulation of ROS is known to accompany protein aggregation, both within the context of neurodegenerative disease-causing proteins, such as mutant huntingtin (26), β -amyloid, and α -synuclein (27), as well as non-disease causing proteins such as the *E. coli*-derived HypF (28). ROS production has been associated with proteasome inhibition in numerous cancer models (35–37), and increased oxidative stress has recently been correlated with improved clinical response to bortezomib in mantle cell lymphoma (38). Even though our data do not identify the exact mechanism(s) by which protein aggregates stimulate ROS production, ROS production correlates closely with cytotoxicity, and the thiol antioxidant NAC blocked both ROS production and cell death. Therefore, ROS production appears to contribute directly to the cytotoxicity of protein aggregates.

The biochemical mechanisms underlying the lack of inducible phosphorylation in our BZ-sensitive cells also remain unresolved (Fig. 7). Our results demonstrating that BZ activated HRI as well in the BZ-sensitive CF-Pac1 cells as it did in the BZ-resistant Suit2 cells (Fig. 5D) indicate that defective eIF2 α kinase activation is likely not the explanation. It is possible that the BZ-sensitive cells experience a chronic stress that causes maximal (saturated) eIF2 α .

phosphorylation mediated by GCN2, thereby preventing further inducible phosphorylation. We have also observed constitutively high levels of autophagy in our BZ-sensitive cell lines that may be linked to this basal stress (data not shown). Indeed, Wengrod et al. (39) recently demonstrated GCN2-eIF2 α -P signaling to be necessary for autophagy induction following mTORC1 inhibition and amino acid starvation in melanoma. This response was controlled by levels of protein phosphatase 6 (PP6C), which forms a complex with GCN2 that is required to phosphorylate eIF2 α . Interestingly, PP6C aberrancies in melanoma may drive higher eIF2 α -P levels and autophagy, a mechanism that may be at play in our BZ-sensitive cell lines. Phospho-eIF2 α levels are linked to better overall survival in lung cancer (40), and our data argue for further exploration of basal eIF2 α phosphorylation as a predictor of sensitivity to proteasome inhibitors and possibly other agents in patients. We plan to investigate the molecular mechanisms contributing to constitutive eIF2 α phosphorylation and autophagy using whole genome expression profiling and other approaches, focusing on the hypothesis that it might be related to some type of underlying metabolic stress. It is also possible that differences in phosphatase expression/activity could be affecting eIF2 α phosphorylation in our pancreatic cancer cells; in addition to PP6C, modulation of either GADD34 (PPP1R15A) or constitutive repressor of eIF2 α phosphorylation (CReP) (PPP1R15B) have been shown to influence phospho-eIF2 α levels (41, 42). Accordingly, preliminary experiments suggest that the BZ-resistant pancreatic cells express higher levels of GADD34 than do the BZ-sensitive cells (data not shown).

Despite an abundance of literature on the effects of proteasome inhibitors in normal and cancer cells, the initial stress elicited by blocking the proteasome remains unclear. ER stress and heat shock responses are both documented consequences of proteasome inhibition (43–45). Here, our quantitative comparison of both ER- and cytosolic stress gene readouts (Fig. 5) strongly suggests that the stress elicited by proteasome inhibition in pancreatic cancer cells may originate within the cytosol and more closely resemble the effects of heat shock rather than ER stress. Although kinetic differences between the timing of HSF1- and UPR-driven responses may exist, our data confirmed that Grp78 and CHOP were modestly upregulated by BZ (46, 47), while Hsp72 mRNA levels increased much more impressively, consistent with activation of a canonical heat shock response; the robust activation of the cytosolic kinase HRI versus the more modest activation of PERK in our cells further supports this hierarchical model of BZ-induced stress (Fig. 5D). Our results implicating HRI in BZ-induced eIF2 α phosphorylation and cytoprotection are consistent with the work of Lu, et al. (48), who concluded that HRI controlled translational attenuation in response to a variety of cytosolic stressors such as arsenite, heat shock, and osmotic stress, but not ER-stress or nutrient starvation. Similarly, HRI was also implicated in the stress response following lead exposure in mammalian cells (49). Like the other eIF2 α kinases, HRI activation is accompanied by extensive autophosphorylation, with the Thr485 residue being most critical for kinase activity (50). Importantly, HRI is sequestered in an inactive state by cytosolic chaperones such as Hsc70/Hsp72 and Hsp90 and activated when the chaperones are competed away by denatured or misfolded proteins (51–53). This mechanism of activation closely resembles the Grp78-dependent regulation of PERK within the ER and provides a plausible mechanism for HRI activation by BZ. Alternatively, BZ-induced oxidative stress could also contribute to HRI activation. Indeed, antioxidants were shown to

temper HRI-driven P-eIF2 α levels following arsenite exposure (48), suggesting HRI may be directly or indirectly activated by oxidative stress. Collectively, our results contrast with a recent study that concluded that proteasome inhibition caused amino acid pool depletion, GCN2-mediated eIF2 α -phosphorylation, and CHOP-dependent apoptosis (54). Although it is likely that proteasome inhibitors do cause some amino acid depletion, we did not observe activation of GCN2 in our cells under conditions that led to clear activation of HRI and PERK. Furthermore, not only was CHOP not required for BZ-induced cell death, knockdown of CHOP caused significant cell death on its own and significantly enhanced the cytotoxic effects of BZ (Supplemental Fig. 2).

Ours is the first study to identify HRI as the BZ-activated eIF2 α kinase in pancreatic cancer models, and our data are consistent with the results of Fournier, et al. (55) who implicated HRI in the BZ-induced formation of stress granules. Whereas other groups have begun activating HRI to sensitize multiple myeloma cells to therapy (56), our data provide a strong rationale for inhibiting HRI as a means of sensitizing pancreatic cancer cells to proteasome inhibitors. Notably, disruption of HRI signaling appears to be well-tolerated *in vivo*, as HRI^{-/-} mice were found to be completely normal and fertile, with only mild hematologic abnormalities (10). Considerable progress has recently been made toward developing specific HRI modulators (57), and our work supports this continued pursuit.

MATERIALS AND METHODS

Cell lines and culture

HPDE immortalized pancreatic ductal epithelial cells were a gift from Dr. Craig Logsdon (Department of Cancer Biology, U.T. M.D. Anderson Cancer Center). BxPC3, Panc1, HS766t, MiaPaCA-2, and CF-Pac1 pancreatic cancer cells were obtained from ATCC (American Type Culture Collection, Manassas, VA). Suit2, SU86.86, and T3M4 pancreatic cancer cells were obtained from Eric Collisson (UCSF). mPanc96 pancreatic cancer cells are a genetically identical but phenotypically distinct variant of AsPC1 cells. The identities of all of the human cell lines were validated by DNA fingerprinting, performed in the MD Anderson Characterized Cancer Cell Line Core. All pancreatic cancer cells (except for BxPC3) were maintained in DMEM supplemented with 10% fetal bovine serum (HyClone/Thermo Scientific, Waltham, MA), MEM vitamins, sodium pyruvate (Mediatech/Corning Cellgro, Manassas, VA), L-glutamine, non-essential amino acids, Penicillin/Streptomycin (Lonza, Switzerland), and HEPES. BxPC3 cells were cultured in RPMI-1640 supplemented with 10% fetal bovine serum (HyClone/Thermo Scientific), MEM vitamins, L-glutamine, sodium pyruvate, non-essential amino acids, Penicillin/Streptomycin, and HEPES. HPDE cells were maintained in serum-free keratinocyte media supplemented with EGF and BPE (Gibco/Life Technologies, Grand Island, NY). Wild-type eIF2 α ^{51SS} and eIF2 α ^{51AA} knock-in mutant MEFs were obtained from Dr. David Ron (NYU/University of Cambridge) and grown as described previously (7). All cells were grown in a humidified incubator at 37° C under an atmosphere of 5% CO₂ in air and periodically checked for mycoplasma contamination.

Chemicals and antibodies

Bortezomib was purchased from ChemieTek (Indianapolis, IN). Thapsigargin, cycloheximide, and propidium iodide (PI) and *N*-acetyl-L-cysteine (NAC) were purchased from Sigma-Aldrich (St. Louis, MO). Antibodies were purchased from the following sources: phospho-eIF2 α (#3398S), GCN2 (#3302), PERK (#3192) and lamin A/C (#4777) (Cell Signaling Technology, Beverly, MA), eIF2 α , (#44-728G, Invitrogen/Life Technologies, Grand Island, NY), HRI (#sc-30143), ubiquitin (#sc-8017) and ATF4 (#sc-200) (Santa Cruz Biotechnology, Santa Cruz, CA), phospho-GCN2 (#ab75836, Abcam, Cambridge, MA), β -actin (#A5316, Sigma-Aldrich), and anti-mouse/anti-rabbit HRP-labeled secondary antibodies (#W4021/#W4011, Promega, Madison, WI).

Immunoblotting

Cells (~70% confluency) were collected via scraping on ice, and lysed by vigorous vortexing using a 1% NP-40 buffer containing 50mM Tris-HCl (pH 7.4), 150mM NaCl, 5mM EDTA, 0.1% Triton X-100, 25mM NaF, 100mM Na₃VO₄, 10mM glycerophosphate, 10mM PMSF, and complete protease inhibitors. Lysates were clarified by centrifugation and then protein concentrations were quantified using a commercial Bradford assay (Bio-Rad, Hercules, CA). Equal amounts of protein (15–20 μ g) were separated by 6–10% SDS-PAGE and transferred to nitrocellulose membranes. Membranes were blocked with either 5% bovine serum albumin (BSA) or 5% nonfat dried milk dissolved in TBS-T, then probed overnight in the same solutions with primary antibodies. Membranes were then washed and incubated with species-specific horseradish peroxidase-labeled secondary antibodies. Immunoblots were developed by chemiluminescence (GE Healthcare Life Sciences, Piscataway, NJ), and densitometry was performed using ImageJ.

Measurement of cell viability

Cells were plated in 6-well plates and allowed to attach overnight. Cells (~40–60% confluency) were then exposed to drugs for 48 hours and collected by trypsinization. Cell pellets were washed once in PBS and then resuspended in 0.5mL of fresh PBS. Propidium-iodide (PI) solution (100 μ g/mL) was added in a 1:10 dilution immediately prior to analyzing the samples. PI-positive (non-viable) cells were measured by FACS (fluorescence activated cell sorting) analysis on the FL3 channel of a Beckman Coulter FC500 flow cytometer.

³H-leucine incorporation assays

Equal numbers of cells were plated in 6-well plates (~2–3 \times 10⁵ cells/well) and allowed to attach overnight. Cells were exposed to bortezomib (30nM) or cycloheximide (20 μ M) as indicated. Following incubation, drugs were removed and cells were pulsed for 1–2 hours with 1 μ Ci/mL L-[4,5- ³H(N)] leucine (Perkin-Elmer, Waltham, MA) in leucine-free media (MP Biomedicals, Solon, OH) supplemented with 10% dialyzed FBS, vitamins, L-glutamine, antibiotics, and HEPES. Cells were trypsinized and pellets lysed in a 1% Triton X-100 buffer containing 25mM Tris-HCl, 300mM NaCl, and 10mM PMSF plus complete protease inhibitors by rotation for 20–30 minutes at 4° C. Lysates were clarified via centrifugation and proteins were precipitated overnight at 4° C in 5% trichloroacetic acid (TCA). The resulting precipitates were collected via centrifugation and dissolved in 0.1%

KOH. Samples were aliquoted in triplicate and combined with scintillation fluid (ThermoFisher Scientific, Waltham, MA). CPMs were measured by a Beckman Coulter LS6500 scintillation counter.

Leucine deprivation

Following overnight attachment, complete DMEM was removed from cells and cells were washed 1x in PBS. Leucine-free media (see above) was added for 2 hours prior to harvesting.

Quantitative real-time PCR

Cells were harvested at ~70% confluency and total RNA was isolated using the *mirVANA* miRNA isolation kit (Ambion/Life Technologies, Grand Island, NY). Final RNA isolates were checked for quality and concentration using a NanoDrop ND-1000 spectrophotometer (NanoDrop/ThermoFisher Scientific). Specific primers for GRP78, CHOP, and HSPA1A (Applied Biosystems/Life Technologies) were amplified by Taqman-based one-step real-time PCR (Ambion/Life Technologies; ABI 7900HT Fast Real-Time PCR System).

Immunofluorescence

Cells were plated on either 4-well (50,000 cells/well) or 8-well (20,000 cells/well) chamber slides and allowed to attach overnight. Following drug exposure, cells were fixed and permeabilized with either acetone or 4% paraformaldehyde and 100 μ g/mL digitonin. Slides were blocked in 5% horse serum and 1% goat serum and then the primary antibody was added overnight. Fluorescent secondary antibodies, Cy3 or DyLight 549 anti-mouse (Jackson Immunoresearch Labs, West Grove, PA) were added for 1 hour at room temperature. Nuclei were counterstained with a 1:10,000 dilution of Sytox Green and coverslips mounted using propyl gallate. Cells were imaged using a Zeiss Axioplan 2 fluorescent microscope mounted with a Hamamatsu ORCA-ER camera.

Detergent-insoluble protein aggregates assay

Cells (50–70% confluency) were exposed to bortezomib for 24 hours and collected via scraping on ice. Cells were lysed by gentle rotation for 15 minutes at 4°C in the 1% Triton X-100 buffer described previously. Detergent-soluble and -insoluble fractions were isolated by centrifugation at maximum speed (16,000 $\times g$) for 15 minutes. The resulting supernatants were saved as the detergent-soluble fraction, while the resulting pellets were resuspended in a 6M urea-containing sample buffer by sonication for 15 seconds and saved as the detergent-insoluble fractions. Proteins were resolved by 10% SDS-PAGE and membranes probed with an anti-ubiquitin antibody. Densitometry was performed using ImageJ.

Measurement of reactive oxygen species (ROS)

Cells (50–70% confluency) were plated in 6-well plates and allowed to attach overnight. Where indicated, 10 mM NAC was added 1 hour prior to bortezomib exposure. Cells were then exposed to bortezomib for 18 hours. One hour prior to harvesting, 1 μ M of the redox-sensitive dye 2',7'-dichlorodihydro-fluorescein diacetate (H₂DCFDA) (Invitrogen/Life Technologies, Grand Island, NY) was added to each well. Cells were then collected by

trypsinization and washed 1x in cold PBS. H₂DCFDA fluorescence was measured on the FL1 channel of a Beckman Coulter FC500 cytometer. Histogram overlays were generated using FlowJo software (Tree Star, Inc., Ashland, OR).

siRNA-mediated gene silencing assays

Cells were transfected with ON-TARGETplus SMARTpool siRNAs specific for GCN2, HRI, PERK, PKR, CHOP or a non-targeting control (Dharmacon RNAi Technologies/GE Life Sciences). All targets were silenced via the reverse-transfection protocol included with the RNAiMAX transfection reagent (Invitrogen/Life Technologies) for 48–72 hours before exposing cells to drug. Target-specific knockdown efficiency was verified by quantitative RT-PCR and immunoblotting.

shRNA-mediated gene silencing assays

Cells were transduced with pGIPZ lentiviral vectors containing shRNA specific for either HRI (EIF2AK1), GCN (EIF2AK4), or a nonspecific control (Dharmacon RNAi Technologies/GE Life Sciences). Oligo ID information is as follows: HRI-A (V2LHS_1500), HRI-B (V3LHS_638761), HRI-C (V3LHS_638768), GCN2-A (V2LHS_202539), GCN2-B (V3LHS_350194), GCN2-C (V3LHS_350196). Stably transduced cells were selected using 10 μ g/mL of puromycin (Gibco/ThermoFisher Scientific).

Statistics

Statistical analyses were performed using two-sided Student's *t* test functions from GraphPad Prism 5 software and Microsoft Excel. A normal distribution was assumed. Results represent data from independent experiments performed in duplicate at a minimum, with specific sample sizes reported in the respective figure legends. Variance was estimated as standard error of the mean (SE) and variances were similar between compared groups. P-values of ≤ 0.05 were considered statistically significant.

Supplementary Material

Refer to Web version on PubMed Central for supplementary material.

Acknowledgments

This work was supported by grants from NIH/NCI (R01 CA127494), and the M.D. Anderson Cancer Center Support Grant P30 CA016672-38 (D.J.M.). M.C.W. would like to acknowledge awards from The Albert Schweitzer Fellowship and the Tzu-Chi Foundation

References

1. Adams J, Kauffman M. Development of the proteasome inhibitor Velcade (Bortezomib). *Cancer Invest.* 2004; 22(2):304–11. [PubMed: 15199612]
2. Goldberg AL. Probing the proteasome pathway. *Nat Biotechnol.* 2000; 18(5):494–6. [PubMed: 10802613]
3. Jiang HY, Wek RC. Phosphorylation of the alpha-subunit of the eukaryotic initiation factor-2 (eIF2alpha) reduces protein synthesis and enhances apoptosis in response to proteasome inhibition. *J Biol Chem.* 2005; 280(14):14189–202. [PubMed: 15684420]

4. Yerlikaya A, Kimball SR, Stanley BA. Phosphorylation of eIF2alpha in response to 26S proteasome inhibition is mediated by the haem-regulated inhibitor (HRI) kinase. *Biochem J.* 2008; 412(3):579–88. [PubMed: 18290760]
5. Obeng EA, Carlson LM, Gutman DM, Harrington WJ Jr, Lee KP, Boise LH. Proteasome inhibitors induce a terminal unfolded protein response in multiple myeloma cells. *Blood.* 2006; 107(12):4907–16. [PubMed: 16507771]
6. Lee DH, Goldberg AL. Proteasome inhibitors cause induction of heat shock proteins and trehalose, which together confer thermotolerance in *Saccharomyces cerevisiae*. *Mol Cell Biol.* 1998; 18(1): 30–8. [PubMed: 9418850]
7. Zhu K, Dunner K Jr, McConkey DJ. Proteasome inhibitors activate autophagy as a cytoprotective response in human prostate cancer cells. *Oncogene.* 2010; 29(3):451–62. [PubMed: 19881538]
8. Baird TD, Wek RC. Eukaryotic initiation factor 2 phosphorylation and translational control in metabolism. *Adv Nutr.* 2012; 3(3):307–21. [PubMed: 22585904]
9. Harding HP, Zhang Y, Zeng H, Novoa I, Lu PD, Calfon M, et al. An Integrated Stress Response Regulates Amino Acid Metabolism and Resistance to Oxidative Stress. *Molecular Cell.* 2003; 11(3): 619–33. [PubMed: 12667446]
10. Han AP, Yu C, Lu L, Fujiwara Y, Browne C, Chin G, et al. Heme-regulated eIF2alpha kinase (HRI) is required for translational regulation and survival of erythroid precursors in iron deficiency. *EMBO J.* 2001; 20(23):6909–18. [PubMed: 11726526]
11. Zhang F, Romano PR, Nagamura-Inoue T, Tian B, Dever TE, Mathews MB, et al. Binding of double-stranded RNA to protein kinase PKR is required for dimerization and promotes critical autophosphorylation events in the activation loop. *J Biol Chem.* 2001; 276(27):24946–58. [PubMed: 11337501]
12. Walter P, Ron D. The unfolded protein response: from stress pathway to homeostatic regulation. *Science.* 2011; 334(6059):1081–6. [PubMed: 22116877]
13. Wek SA, Zhu S, Wek RC. The histidyl-tRNA synthetase-related sequence in the eIF-2 alpha protein kinase GCN2 interacts with tRNA and is required for activation in response to starvation for different amino acids. *Mol Cell Biol.* 1995; 15(8):4497–506. [PubMed: 7623840]
14. Taniuchi S, Miyake M, Tsugawa K, Oyadomari M, Oyadomari S. Integrated stress response of vertebrates is regulated by four eIF2alpha kinases. *Sci Rep.* 2016; 6:32886. [PubMed: 27633668]
15. Balch WE, Morimoto RI, Dillin A, Kelly JW. Adapting proteostasis for disease intervention. *Science.* 2008; 319(5865):916–9. [PubMed: 18276881]
16. Ross CA, Poirier MA. Protein aggregation and neurodegenerative disease. *Nature Medicine.* 2004; 10(7):S10–S7.
17. Jones RG, Thompson CB. Tumor suppressors and cell metabolism: a recipe for cancer growth. *Genes Dev.* 2009; 23(5):537–48. [PubMed: 19270154]
18. Solimini NL, Luo J, Elledge SJ. Non-oncogene addiction and the stress phenotype of cancer cells. *Cell.* 2007; 130(6):986–8. [PubMed: 17889643]
19. Xu W, Trepel J, Neckers L. Ras, ROS and proteotoxic stress: a delicate balance. *Cancer Cell.* 2011; 20(3):281–2. [PubMed: 21907917]
20. Chauhan D, Hideshima T, Anderson KC. Proteasome inhibition in multiple myeloma: therapeutic implication. *Annu Rev Pharmacol Toxicol.* 2005; 45:465–76. [PubMed: 15822185]
21. Kane RC, Dagher R, Farrell A, Ko CW, Sridhara R, Justice R, et al. Bortezomib for the treatment of mantle cell lymphoma. *Clin Cancer Res.* 2007; 13(18 Pt 1):5291–4. [PubMed: 17875757]
22. Nawrocki ST, Carew JS, Pino MS, Highshaw RA, Andtbacka RH, Dunner K Jr, et al. Aggresome disruption: a novel strategy to enhance bortezomib-induced apoptosis in pancreatic cancer cells. *Cancer Res.* 2006; 66(7):3773–81. [PubMed: 16585204]
23. Zhu K, Chan W, Heymach J, Wilkinson M, McConkey DJ. Control of HIF-1alpha expression by eIF2 alpha phosphorylation-mediated translational repression. *Cancer Res.* 2009; 69(5):1836–43. [PubMed: 19244104]
24. Knutsen JH, Rodland GE, Boe CA, Haland TW, Sunnerhagen P, Grallert B, et al. Stress-induced inhibition of translation independently of eIF2alpha phosphorylation. *J Cell Sci.* 2015; 128(23): 4420–7. [PubMed: 26493332]

25. Leu JI, Pimkina J, Frank A, Murphy ME, George DL. A small molecule inhibitor of inducible heat shock protein 70. *Molecular cell*. 2009; 36(1):15–27. [PubMed: 19818706]
26. Wyttenbach A, Sauvageot O, Carmichael J, Diaz-Latoud C, Arrigo AP, Rubinsztein DC. Heat shock protein 27 prevents cellular polyglutamine toxicity and suppresses the increase of reactive oxygen species caused by huntingtin. *Hum Mol Genet*. 2002; 11(9):1137–51. [PubMed: 11978772]
27. Tabner BJ, Turnbull S, El-Agnaf OM, Allsop D. Formation of hydrogen peroxide and hydroxyl radicals from A(beta) and alpha-synuclein as a possible mechanism of cell death in Alzheimer's disease and Parkinson's disease. *Free Radic Biol Med*. 2002; 32(11):1076–83. [PubMed: 12031892]
28. Bucciantini M, Calloni G, Chiti F, Formigli L, Nosi D, Dobson CM, et al. Prefibrillar amyloid protein aggregates share common features of cytotoxicity. *J Biol Chem*. 2004; 279(30):31374–82. [PubMed: 15133040]
29. Jenner P. Oxidative stress in Parkinson's disease. *Annals of neurology*. 2003; 53(Suppl 3):S26–36. discussion S-8. [PubMed: 12666096]
30. Wu D, Yotnda P. Production and detection of reactive oxygen species (ROS) in cancers. *J Vis Exp*. 2011(57)
31. Chen S, Blank JL, Peters T, Liu XJ, Rappoli DM, Pickard MD, et al. Genome-wide siRNA screen for modulators of cell death induced by proteasome inhibitor bortezomib. *Cancer Res*. 2010; 70(11):4318–26. [PubMed: 20460535]
32. Meister S, Schubert U, Neubert K, Herrmann K, Burger R, Gramatzki M, et al. Extensive Immunoglobulin Production Sensitizes Myeloma Cells for Proteasome Inhibition. *Cancer Research*. 2007; 67(4):1783–92. [PubMed: 17308121]
33. Schewe DM, Aguirre-Ghiso JA. Inhibition of eIF2alpha dephosphorylation maximizes bortezomib efficiency and eliminates quiescent multiple myeloma cells surviving proteasome inhibitor therapy. *Cancer Res*. 2009; 69(4):1545–52. [PubMed: 19190324]
34. Vilas-Boas Fde A, da Silva AM, de Sousa LP, Lima KM, Vago JP, Bittencourt LF, et al. Impairment of stress granule assembly via inhibition of the eIF2alpha phosphorylation sensitizes glioma cells to chemotherapeutic agents. *J Neurooncol*. 2016; 127(2):253–60. [PubMed: 26732083]
35. Miller CP, Ban K, Dujka ME, McConkey DJ, Munsell M, Palladino M, et al. NPI-0052, a novel proteasome inhibitor, induces caspase-8 and ROS-dependent apoptosis alone and in combination with HDAC inhibitors in leukemia cells. *Blood*. 2007; 110(1):267–77. [PubMed: 17356134]
36. Ling YH, Liebes L, Zou Y, Perez-Soler R. Reactive oxygen species generation and mitochondrial dysfunction in the apoptotic response to Bortezomib, a novel proteasome inhibitor, in human H460 non-small cell lung cancer cells. *J Biol Chem*. 2003; 278(36):33714–23. [PubMed: 12821677]
37. Perez-Galan P, Roue G, Villamor N, Montserrat E, Campo E, Colomer D. The proteasome inhibitor bortezomib induces apoptosis in mantle-cell lymphoma through generation of ROS and Noxa activation independent of p53 status. *Blood*. 2006; 107(1):257–64. [PubMed: 16166592]
38. Weniger MA, Rizzatti EG, Perez-Galan P, Liu D, Wang Q, Munson PJ, et al. Treatment-induced oxidative stress and cellular antioxidant capacity determine response to bortezomib in mantle cell lymphoma. *Clin Cancer Res*. 2011; 17(15):5101–12. [PubMed: 21712452]
39. Wengrod J, Wang D, Weiss S, Zhong H, Osman I, Gardner LB. Phosphorylation of eIF2alpha triggered by mTORC1 inhibition and PP6C activation is required for autophagy and is aberrant in PP6C-mutated melanoma. *Sci Signal*. 2015; 8(367):ra27. [PubMed: 25759478]
40. He Y, Correa AM, Raso MG, Hofstetter WL, Fang B, Behrens C, et al. The role of PKR/eIF2alpha signaling pathway in prognosis of non-small cell lung cancer. *PLoS One*. 2011; 6(11):e24855. [PubMed: 22102852]
41. Moreno JA, Radford H, Peretti D, Steinert JR, Verity N, Martin MG, et al. Sustained translational repression by eIF2alpha-P mediates prion neurodegeneration. *Nature*. 2012; 485(7399):507–11. [PubMed: 22622579]
42. Jousse C, Oyadomari S, Novoa I, Lu P, Zhang Y, Harding HP, et al. Inhibition of a constitutive translation initiation factor 2alpha phosphatase, CREP, promotes survival of stressed cells. *J Cell Biol*. 2003; 163(4):767–75. [PubMed: 14638860]

43. Kawazoe Y, Nakai A, Tanabe M, Nagata K. Proteasome inhibition leads to the activation of all members of the heat-shock-factor family. *Eur J Biochem.* 1998; 255(2):356–62. [PubMed: 9716376]
44. Bush KT, Goldberg AL, Nigam SK. Proteasome inhibition leads to a heat-shock response, induction of endoplasmic reticulum chaperones, and thermotolerance. *J Biol Chem.* 1997; 272(14): 9086–92. [PubMed: 9083035]
45. Fribley A, Zeng Q, Wang CY. Proteasome inhibitor PS-341 induces apoptosis through induction of endoplasmic reticulum stress-reactive oxygen species in head and neck squamous cell carcinoma cells. *Mol Cell Biol.* 2004; 24(22):9695–704. [PubMed: 15509775]
46. Nawrocki ST, Carew JS, Dunner K Jr, Boise LH, Chiao PJ, Huang P, et al. Bortezomib inhibits PKR-like endoplasmic reticulum (ER) kinase and induces apoptosis via ER stress in human pancreatic cancer cells. *Cancer Res.* 2005; 65(24):11510–9. [PubMed: 16357160]
47. Nawrocki ST, Carew JS, Pino MS, Highshaw RA, Dunner K Jr, Huang P, et al. Bortezomib sensitizes pancreatic cancer cells to endoplasmic reticulum stress-mediated apoptosis. *Cancer Res.* 2005; 65(24):11658–66. [PubMed: 16357177]
48. Lu L, Han AP, Chen JJ. Translation initiation control by heme-regulated eukaryotic initiation factor 2alpha kinase in erythroid cells under cytoplasmic stresses. *Mol Cell Biol.* 2001; 21(23):7971–80. [PubMed: 11689689]
49. Mittal SP, Kulkarni AP, Mathai J, Chattopadhyay S, Pal JK. Dose-dependent differential response of mammalian cells to cytoplasmic stress is mediated through the heme-regulated eIF2alpha kinase. *The international journal of biochemistry & cell biology.* 2014; 54:186–97. [PubMed: 25086227]
50. Rafie-Kolpin M, Han AP, Chen JJ. Autophosphorylation of threonine 485 in the activation loop is essential for attaining eIF2alpha kinase activity of HRI. *Biochemistry.* 2003; 42(21):6536–44. [PubMed: 12767237]
51. Matts RL, Xu Z, Pal JK, Chen JJ. Interactions of the heme-regulated eIF-2 alpha kinase with heat shock proteins in rabbit reticulocyte lysates. *J Biol Chem.* 1992; 267(25):18160–7. [PubMed: 1355482]
52. Matts RL, Hurst R, Xu Z. Denatured proteins inhibit translation in hemin-supplemented rabbit reticulocyte lysate by inducing the activation of the heme-regulated eIF-2 alpha kinase. *Biochemistry.* 1993; 32(29):7323–8. [PubMed: 8101730]
53. Uma S, Thulasiraman V, Matts RL. Dual role for Hsc70 in the biogenesis and regulation of the heme-regulated kinase of the alpha subunit of eukaryotic translation initiation factor 2. *Mol Cell Biol.* 1999; 19(9):5861–71. [PubMed: 10454533]
54. Suraweera A, Munch C, Hanssum A, Bertolotti A. Failure of amino acid homeostasis causes cell death following proteasome inhibition. *Mol Cell.* 2012; 48(2):242–53. [PubMed: 22959274]
55. Fournier MJ, Gareau C, Mazroui R. The chemotherapeutic agent bortezomib induces the formation of stress granules. *Cancer Cell Int.* 2010; 10:12. [PubMed: 20429927]
56. Burwick N, Zhang MY, de la Puente P, Azab AK, Hyun TS, Ruiz-Gutierrez M, et al. The eIF2-alpha kinase HRI is a novel therapeutic target in multiple myeloma. *Leukemia research.* 2017; 55:23–32. [PubMed: 28119225]
57. Yefidoff-Freedman R, Fan J, Yan L, Zhang Q, Dos Santos GRR, Rana S, et al. Development of 1-((1,4-trans)-4-Aryloxycyclohexyl)-3-arylurea Activators of Heme-Regulated Inhibitor as Selective Activators of the Eukaryotic Initiation Factor 2 Alpha (eIF2alpha) Phosphorylation Arm of the Integrated Endoplasmic Reticulum Stress Response. *J Med Chem.* 2017; 60(13):5392–406. [PubMed: 28590739]

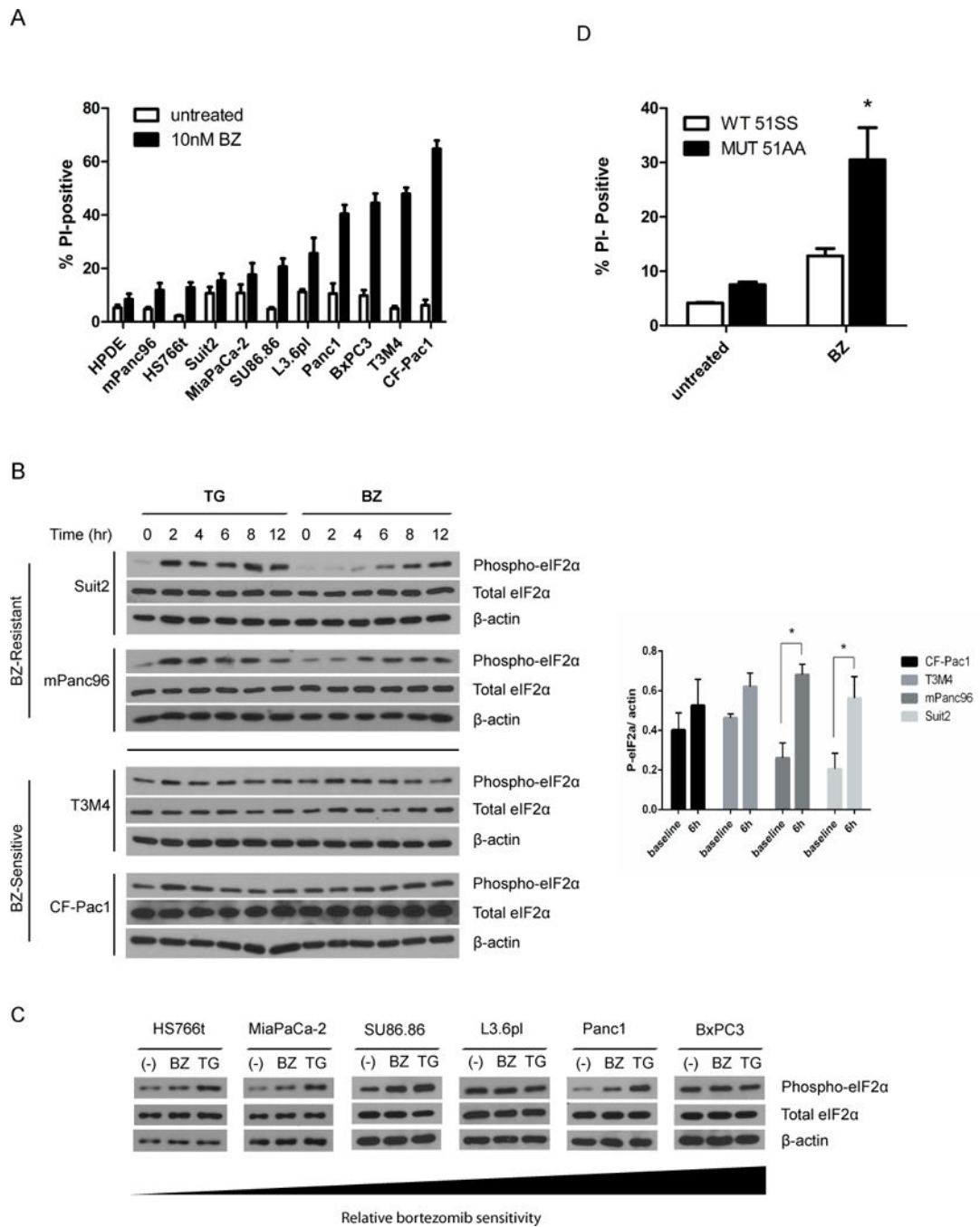


FIGURE 1. Bortezomib sensitivity correlates with defective inducible eIF2 α phosphorylation in human pancreatic cancer cells

A, screen for bortezomib sensitivity in pancreatic cancer cells (BZ). A heterogeneous panel of 10 human pancreatic cancer cell lines and one normal immortalized pancreatic ductal epithelial cell line (HPDE) were exposed to BZ (10nM) for 48 hours and viability measured by PI-uptake/FACS analysis. Columns represent mean \pm SE ($n=3$). *B*, time-course for eIF2 α phosphorylation. BZ-resistant (Suit2, mPanc96) and BZ-sensitive (T3M4, CF-Pac1) cells were exposed to 10 μ M thapsigargin (TG) or 10nM BZ (BZ) for the indicated times and the levels of phosphorylated and total eIF2 α were measured by immunoblotting,

with β -actin serving as a loading control. *C*, densitometry results for phospho- eIF2 α /actin ratios in BZ-sensitive (CF-Pac1, T3M4) and BZ-resistant (mPanc96, Suit2) cells following 6h exposure to 10nM BZ. Columns represent mean \pm SE (n=3). *P \leq 0.05 compared to untreated control columns. *D*, eIF2 α phosphorylation in additional cell lines. Cells were exposed to 10nM BZ for 6 hours (BZ) or 10 μ M thapsigargin for 2 hours (TG) and eIF2 α phosphorylation was measured by immunoblotting. *E*, effects of BZ on cell death in wild-type (51SS) and phosphorylation-deficient mutant (51AA) MEFs. Cells were exposed to 10nM bortezomib (BZ) for 72 hours, and cell viability was measured by PI-uptake/FACS analysis. Columns represent mean \pm SE (n=3). *P $<$ 0.05 compared to wild-type 51SS BZ-treated values.

Author Manuscript

Author Manuscript

Author Manuscript

Author Manuscript

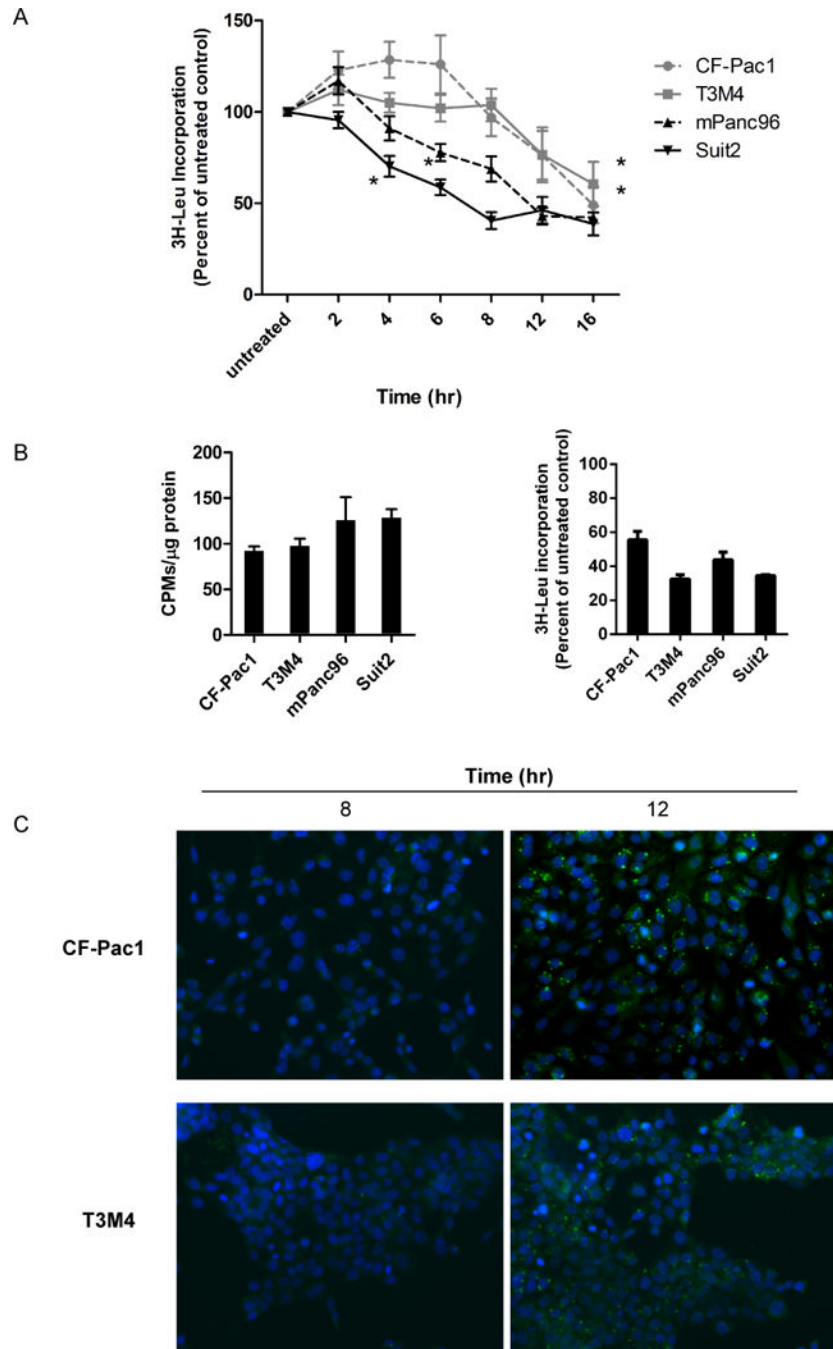


FIGURE 2. Bortezomib-sensitive cells display delayed translation attenuation and form ubiquitin-positive aggregates following exposure to bortezomib

A, measurement of bortezomib (BZ)-induced translational arrest. Left panel, BZ-resistant (Suit2, mPanc96) and BZ-sensitive (CF-Pac1, T3M4) cells were exposed to 30nM bortezomib for the indicated times, and protein synthesis was measured by L-[4,5- 3 H(N)] leucine incorporation. Points represent mean \pm SE (n=4). *Represents time point at which values became significantly different from untreated controls ($P < 0.05$). *B*, control experiments for protein synthesis. Left panel, basal levels of protein synthesis among sensitive (CF-Pac1, T3M4) and resistant (mPanc96, Suit2) cells, normalized to CPMs per μ g

of protein loaded. Right panel, sensitivity of L-[4,5- $^3\text{H}(\text{N})$] leucine incorporation assay validated by cycloheximide, a positive control for inhibition of translation. *C*, measurement of ubiquitin-positive aggregates by immunofluorescent staining. CF-Pac1 and T3M4 were exposed to 10nM BZ as indicated. Blue = nuclear stain; green = ubiquitin. Images are representative of 2 independent experiments.

Author Manuscript

Author Manuscript

Author Manuscript

Author Manuscript

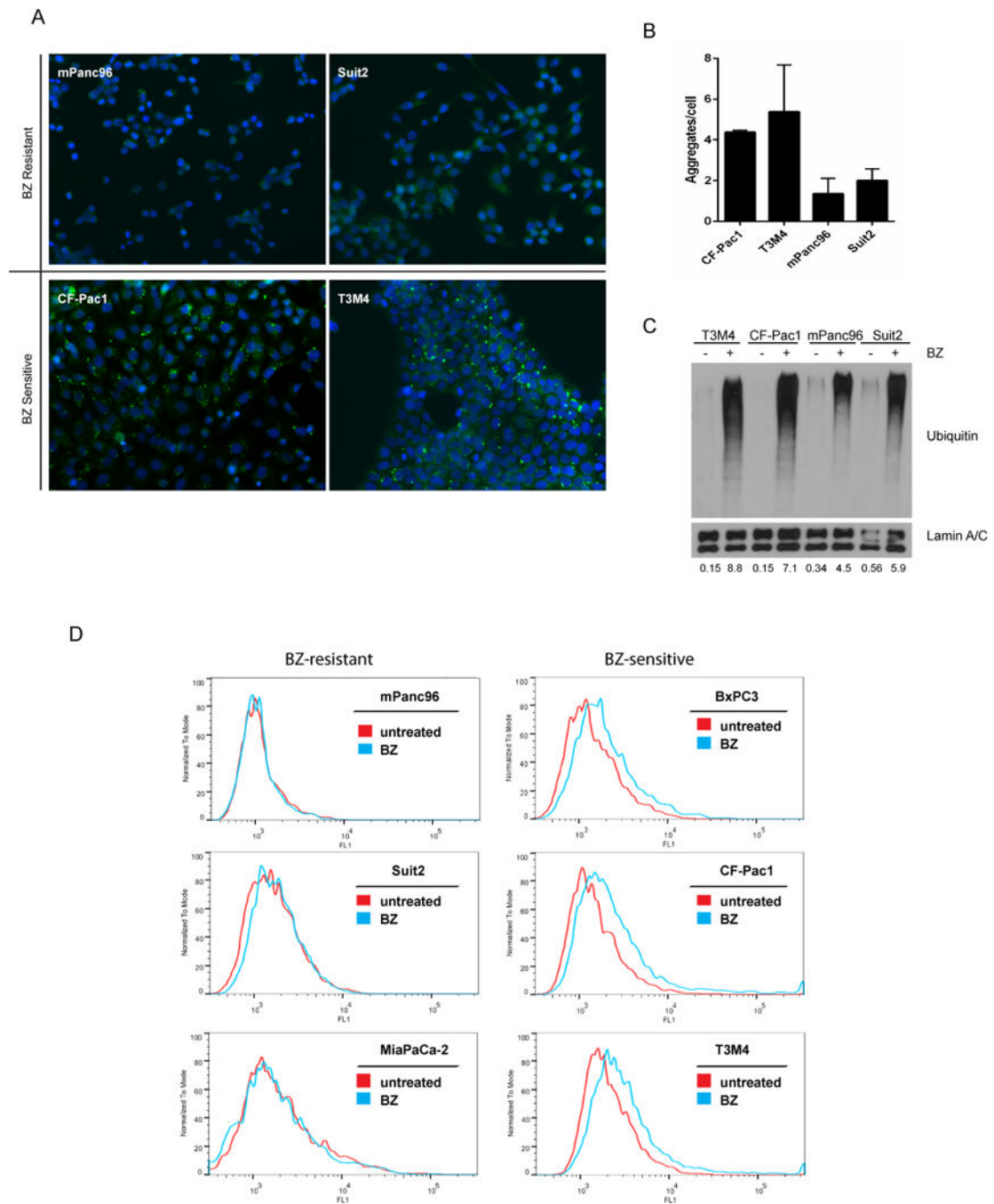


FIGURE 3. Bortezomib-sensitive and –resistant cells display marked differences in bortezomib-induced protein aggregation and generation of reactive oxygen species (ROS)

A, anti-ubiquitin immunofluorescence staining. mPanc96, Suit2, CF-Pac1, and T3M4 were plated in chamber slides and exposed to 10nM BZ for 12h. After fixation, cells were stained for detection of ubiquitin (green) and nuclei (blue). Magnification = 20 \times . Images are representative of 2 independent experiments. *B*, quantification of ubiquitin positive images. Ubiquitin-positive aggregates and nuclei were counted using ImageJ. Columns represent average number of aggregates per cell, \pm SE, ($n=2$, > 150 cells counted in each replicate). *C*, formation of detergent-insoluble protein aggregates. T3M4, CF-Pac1, mPanc96, and Suit2

cells were exposed to 10nM bortezomib (BZ) for 24h, detergent insoluble fractions were isolated, and ubiquitin-positive aggregates were detected by immunoblotting. Lamin A/C served as a loading control. The numbers located below each lane correspond to levels of ubiquitin, as determined by densitometry and with raw values adjusted to lamin A/C levels. Results are representative of 3 independent experiments. *D*, ROS levels in resistant (mPanc96, Suit2, MiaPaCa-2) and sensitive (BxPC3, CF-Pac1, T3M4) cells measured by H₂DCFDA fluorescence (FL1 channel) after an 18 h exposure to 30nM BZ.

Author Manuscript

Author Manuscript

Author Manuscript

Author Manuscript

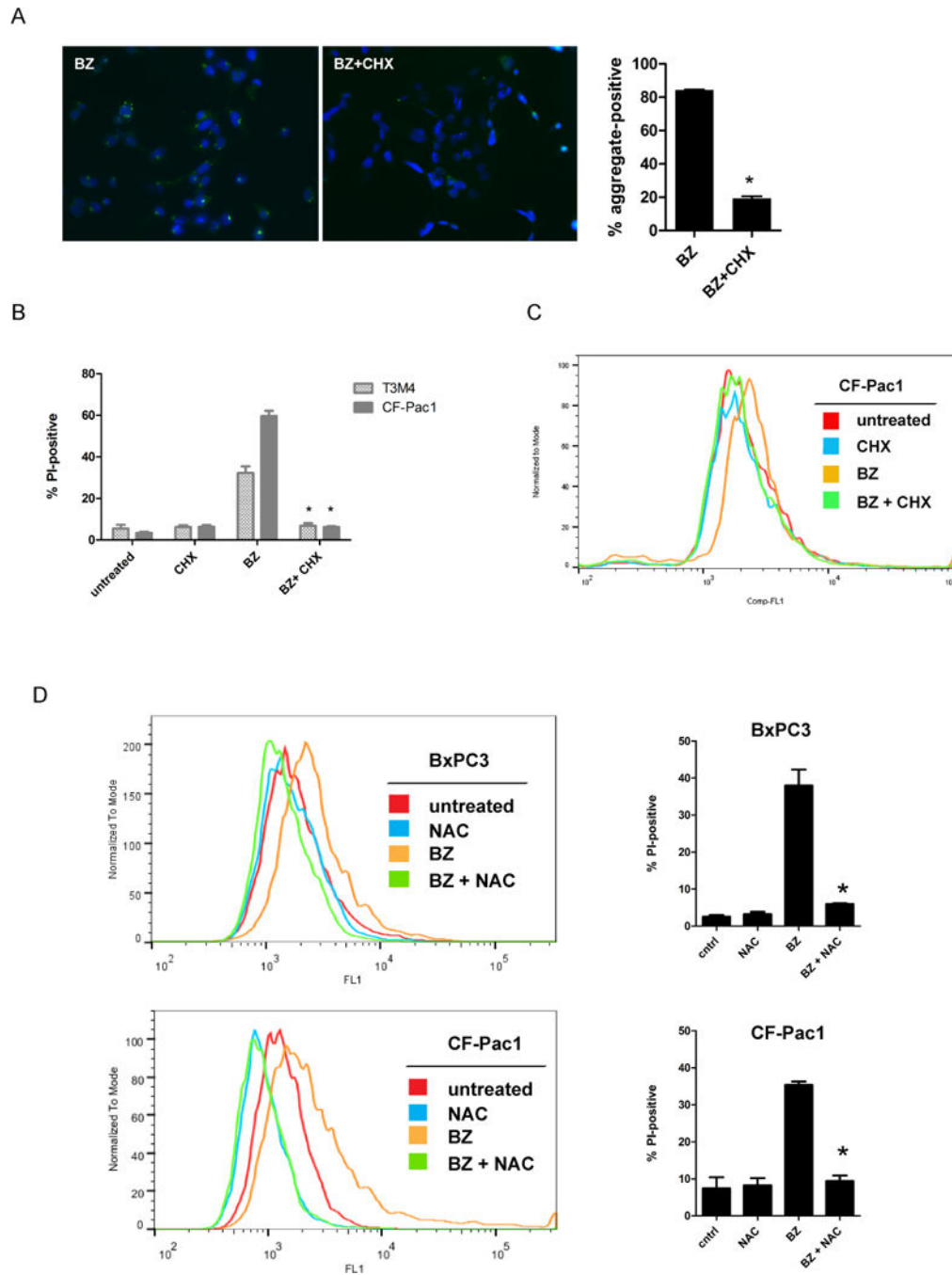


FIGURE 4. Chemical inhibition of translation prevents bortezomib-induced protein aggregation and ROS production, which precipitate cell death

A, anti-ubiquitin immunofluorescence. CF-Pac1 cells with and without a 2 hour pre- incubation with 20 μ M cycloheximide (CHX) were exposed to 30nM bortezomib (BZ) for 24 hours, then fixed and stained. Green represents ubiquitin, blue represents the nuclear stain. Magnification = 20 \times . Right panel, >100 cells from at least 2 representative images from 2 independent experiments were scored for the presence/absence of at least one ubiquitin-positive aggregate. Columns represent mean \pm SE. (n=2). **B**, effects of cycloheximide (CHX) on bortezomib-induced cell death. T3M4 and CF-Pac1 cells with and without a 2 hour

preincubation with 20 μ M CHX were exposed for 48 hours to 30nM BZ as indicated. Cell viability was determined by PI-uptake/FACS analysis. Columns represent mean \pm SE (n=3). *P <0.01 compared with BZ alone. *C*, Pre-treatment with 20 μ M CHX blocks BZ-induced ROS production following an 18h exposure to 30nM BZ. *D*, Left panel, pre-treatment with 10mM of the antioxidant *N*-acetyl-L-cysteine (NAC) blocks ROS production following an 18 hour exposure to 30nM BZ in two sensitive cell lines, BxPC3 and CF-Pac1. Right panel, pre-treatment with 10mM NAC blocks BZ-induced cell death in the corresponding cell lines (48 hour exposure to 30nM BZ). Columns represent mean \pm SE (n=3). *P < 0.02 compared to BZ column.

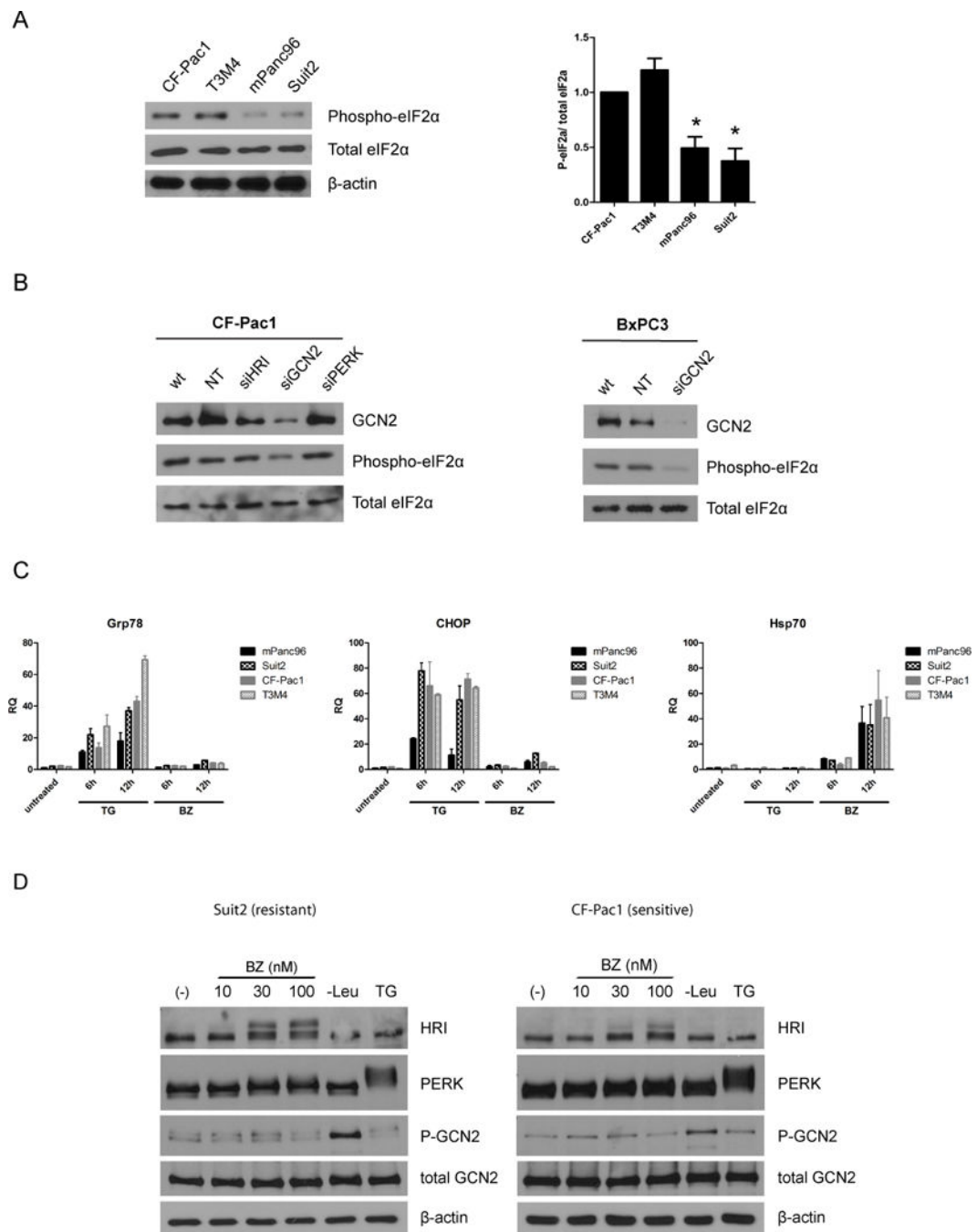


FIGURE 5. Identification of the eIF2 α kinases responsible for both basal and bortezomib-induced eIF2 α phosphorylation in human pancreatic cancer cells

A, Left panel, analysis of basal phospho- eIF2 α levels among sensitive (CF-Pac1, T3M4) and resistant (mPanc96, Suit2) cell lines. Untreated lysates were analyzed for phospho- and total eIF2 α levels by immunoblotting. Right panel, quantification of basal phospho-/total ratios for eIF2 α via densitometry. Columns represent mean \pm SE (n=6). *P < 0.001, compared with CF-Pac1 and T3M4. **B**, effects of silencing eIF2 α kinases on basal phospho-eIF2 α levels. CF-Pac1 cells (left panel) were transfected with siRNAs specific for HRI, GCN2, or PERK, or a non-targeting control siRNA (NT). BxPC3 cells (right panel) were

transfected with siRNA specific for GCN2 or a non-targeting control siRNA (NT). *C*, Effects of BZ on biomarkers of cytosolic or ER stress. Left panel, effects on the ER stress marker Grp78/BiP; middle panel, effects on the ER stress marker CHOP/GADD153; right panel, effects on the cytosolic stress marker Hsp72. mPanc96, Suit2, CF-Pac1, and T3M4 cells were exposed to 10 μ M thapsigargin (TG) or 10nM bortezomib (BZ) as indicated. Expression levels were determined by one-step quantitative RT-PCR. RQ, relative quantity as normalized to the internal control (cyclophilin A). Columns represent mean \pm SE (n=3). *D*, analysis of HRI, PERK, and GCN2 activation following bortezomib exposure. Suit2 and CF-Pac1 cells were either exposed to indicated concentrations of bortezomib (BZ) for 6 hours, leucine-starved for 2 hours, or exposed to 10 μ M thapsigargin (TG) for 2 hours. Phosphorylated and total kinase levels were measured by immunoblotting.

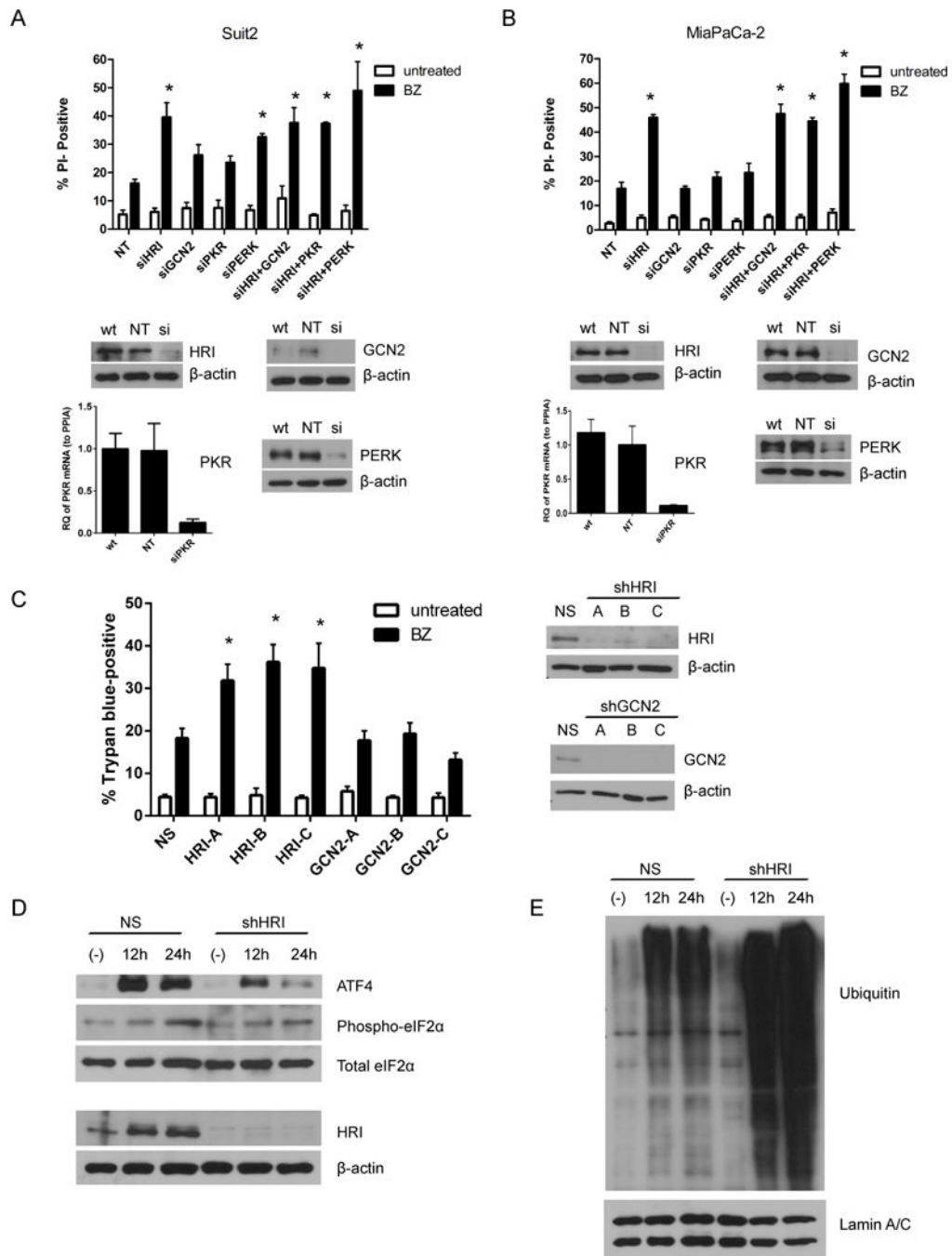


FIGURE 6. Targeting HRI in bortezomib-resistant cells exacerbates proteotoxicity and enhances cell death

A, B, siRNA screen examining the effects of eIF2 α kinase knockdown on bortezomib sensitivity. Suit2 (*A*) and MiaPaCa-2 (*B*) cells were transfected with siRNAs specific for HRI, GCN2, PKR, or PERK, as well as a non-targeting (NT) control siRNA for 48–72 hours. The cells were then exposed to 30nM bortezomib (BZ) for 48 hours, and cell viability was measured by PI-uptake/FACS analysis. Columns represent mean \pm SE ($n=3$). * $P < 0.05$ compared to NT BZ-treated values. Confirmation of HRI, GCN2, and PERK knockdown was done by immunoblotting; PKR knockdown was confirmed by RT-PCR. Results are

representative of duplicate experiments. *C*, stable lentiviral knockdown of HRI and GCN2 in Suit2 cells. Cells were transduced with a lentiviral vector (pGIPZ) containing either a nonspecific (NS) sequence or one of three distinct targeted shRNAs (A,B,C) for both HRI and GCN2. Knockdown was confirmed by immunoblotting (representative of n=2). The cells were then exposed to 30nM BZ for 48 hours, and viability was measured by Trypan Blue staining. Columns represent mean \pm SE (n=5). *P < 0.05 compared to NS BZ-treated values. *D*, Left panel, comparison of Suit2 NS and shHRI cells (B clone) with respect to phospho-eIF2 α and ATF4 levels. Cells were exposed for 12 or 24 hours to 10nM BZ and then probed for ATF4, phospho/total eIF2 α , HRI, and actin. Right panel, detergent-insoluble fraction ubiquitin staining in Suit2 NS and shHRI cells (B clone) following exposure to BZ. Cells were exposed for 12 or 24 hours to 10nM BZ and then detergent-insoluble fractions were prepared and probed for ubiquitin or lamin A/C via immunoblotting.

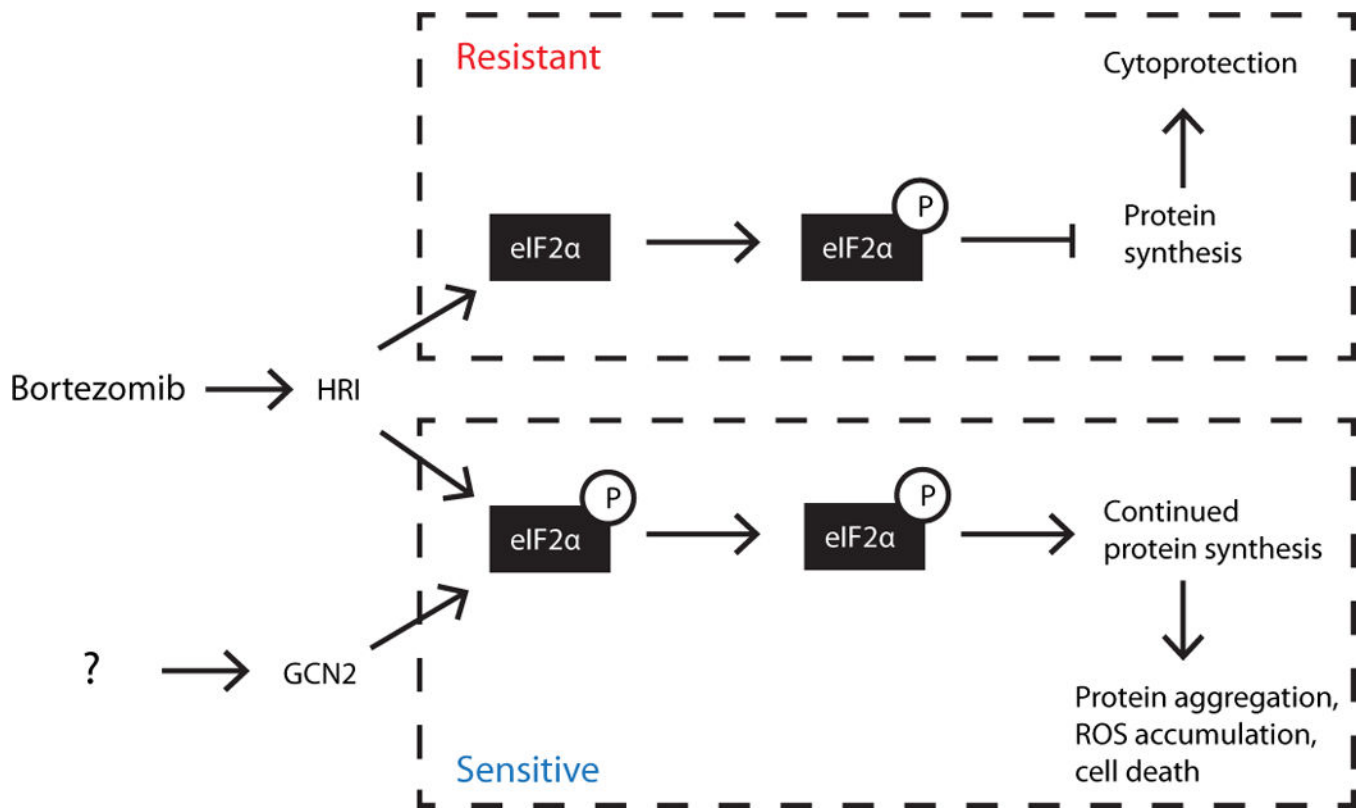


FIGURE 7. Overall scheme outlining the centrality of inducible eIF2 α phosphorylation in determining cellular response to bortezomib

The top half of the figure diagrams an intact phospho- eIF2 α response following bortezomib exposure, in which activated HRI increases levels of phospho-eIF2 α thereby repressing protein synthesis and protecting the cell. The bottom half diagrams the lack of inducible eIF2 α phosphorylation seen in our BZ-sensitive cells, where HRI activation is unable to further phosphorylate eIF2 α , and protein synthesis continues, ultimately leading to toxic accumulations of protein aggregates and ROS. Further investigation is needed to understand what mechanism(s) are promoting the GCN2-mediated, constitutive phosphorylation of eIF2 α in the BZ-sensitive cells.